

Chapter 12

Determination of Constitutive Properties in Inverse Problem Using Airy Stress Function

A. Alshaya, John M. Considine, and R. Rowlands

Abstract A new inverse problem formulation is developed using the Airy stress function. Inverse methods are used to determine the constitutive properties of a graphite/epoxy laminated composite loaded vertically by processing measured values of v -displacement component with an Airy stress function in complex variables. Displacements are recorded using digital image correlation. The traction-free conditions on the symmetrically located sided notches are satisfied analytically using conformal mappings and analytic continuation. The traction-free on the vertical free edge and a symmetrical condition on horizontal line of symmetry are imposed discretely. The primary advantage of this new formulation is the direct use of displacement data, eliminating the need for numerical differentiation when strain data is required. The inverse method algorithm determined the constitutive properties with errors range from 2% to 10%. Selection of Airy coefficients, test geometry configuration and comparison with other inverse methods will be addressed.

Keywords Composites • Airy stress function • Inverse problems • Digital image correlation • Complex variables

12.1 Introduction

The Airy stress function in complex variables was used extensively in determining stresses from measured displacements [1–4]. The Airy stress function can be processed with other measured data using thermoelasticity [5–7], photoelasticity [8], digital image correlation [2], moiré [9] or strain gages [10]. These hybrid methods do not necessitate knowing the applied loads, smooths the measured data and determines individual stresses throughout, including on the edge of the hole. All of the prior applications of the mapping technique evaluated the stresses by using the constitutive properties found experimentally from standard tensile tests whereas the present approach only evaluated these properties using the measured displacement from Digital Image Correlation.

One method of evaluating constitutive properties of orthotropic materials is the use of inverse methods (IM). Avril and Pierron [11] reviewed several IM approaches and showed their general equivalency. IM can be generally described as the iterative adjustments of parameters (constitutive properties) in a numerical model (Airy stress function scheme) to minimize the difference between an experimentally measured quantity (displacement) and the numerically calculated quantity.

By comparing FEM calculated out-of-plane displacement with those measured by shadow moiré, Le Magorou et al. [12] determined bending/torsion rigidities in composite wood panels by the resolution of IM. Molimard et al. [13] evaluated constitutive properties of a composite material by minimizing the difference between moiré-measured displacements and those predicted by FEM in a perforated tensile plate. Similarly, Genovese et al. [14] used IM procedures to evaluate a truss system and a composite plate. Considine [15] determined material properties in heterogeneous materials from full-field simulated displacement data using IM. Each of these references incorporated a specific type of IM entitled FEMU-U (finite element method updating – displacement). The root mean square of displacement differences, also called a cost function, between the measured values and those predicted by FEM are minimized by iteratively changing constitutive properties in

A. Alshaya (✉)
Kuwait University, Kuwait, Kuwait
e-mail: alshaya@wisc.edu

J.M. Considine
Materials Research Engineer, U.S. Forest Service, Forest Products Laboratory, One Gifford Pinchot Drive, Madison, WI 53726, USA
e-mail: jconsidine@wisc.edu

R. Rowlands
University of Wisconsin-Madison, Madison, WI, USA

the FEM model. FEMU-U is attractive because displacements are first-order outputs of high-resolution full-field techniques of DIC and ESPI where strain is a second-order output and has greater noise associated with numerical differentiation.

In 2-D models, the degree of freedom is $(\text{number of nodes}) \times 2 - (\text{number of constitutive parameters}) - 1$. For homogeneous, isotropic materials, the number of constitutive properties is two (E, ν); for homogeneous, orthotropic materials, the number of constitutive parameters are four ($E_{11}, E_{22}, G_{12}, \nu_{12}$). For either case, the number of degrees of freedom is large and the problem is solved by minimizing least squares of the chosen cost function. The goal of this work is to evaluate the constitutive properties of a composite plate containing symmetrically-located sided-notches and vertically loaded in the strongest/stiffest material direction using IM and Airy stress function scheme. The authors are unaware of prior utilization of mapping and complex variables to experimentally determine the constitutive properties in notched composites from displacement data.

12.2 Relevant Equations

For plane problems having rectilinear orthotropy and no body forces, the Airy stress function, F , can be expressed as a summation of two arbitrary analytical functions, $F_1(z_1)$ and $F_2(z_2)$, of the complex variables, z_1 and z_2 , as [13]

$$\mathcal{F} = 2\text{Re}[F_1(z_1) + F_2(z_2)] \quad (12.1)$$

such that $z_j = x + \mu_j y$ for $j = 1, 2$ and Re denotes the ‘real part’ of a complex number. The complex material properties μ_1 and μ_2 depend on the constitutive properties. The displacements in rectangular coordinates (x, y) of the physical $z(=x + iy)$ plane can be expressed in terms of the stress functions. By introducing the new stress functions

$$\Phi(z_1) = \frac{dF_1(z_1)}{dz_1}, \quad \text{and} \quad \Psi(z_2) = \frac{dF_2(z_2)}{dz_2} \quad (12.2)$$

one can write the displacements as

$$u = 2\text{Re}[p_1\Phi(z_1) + p_2\Psi(z_2)] - w_o y + u_o \quad (12.3)$$

$$v = 2\text{Re}[q_1\Phi(z_1) + q_2\Psi(z_2)] + w_o y + v_o \quad (12.4)$$

where w_o, u_o , and v_o are constants of integration and characterize any rigid body translations (u_o and v_o) and rotation (w_o). The other quantities, which depend on material properties, are

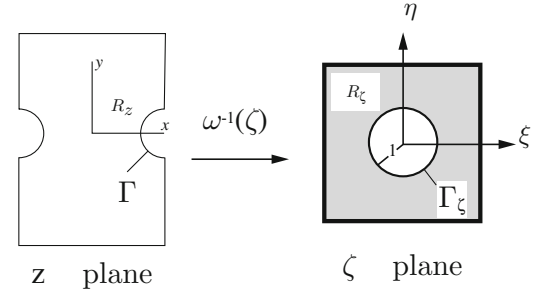
$$p_1 = \frac{\mu_1^2}{E_{11}} - \frac{\nu_{12}}{E_{11}}, \quad p_2 = \frac{\mu_2^2}{E_{11}} - \frac{\nu_{12}}{E_{11}}, \quad q_1 = -\frac{\nu_{12}}{E_{11}}\mu_1 + \frac{1}{E_{22}\mu_1}, \quad q_2 = -\frac{\nu_{12}}{E_{11}}\mu_2 + \frac{1}{E_{22}\mu_2} \quad (12.5)$$

When the plate is loaded physically in a testing machine, the rigid body motions, u_o, v_o , and w_o are zero. Plane problems of elasticity classically involve determining the stress functions, $\Phi(z_1)$ and $\Psi(z_2)$, throughout a component and subject to the boundary conditions around its entire edge. For a region of a component adjacent to a traction free-edge, $\Phi(z_1)$ and $\Psi(z_2)$ can be related to each other by the conformal mapping and analytic continuation techniques. The displacements can then be expressed in terms of the single stress function, $\Phi(z_1)$. Moreover, $\Phi(z_1)$ will be represented by a truncated power-series expansion whose unknown complex coefficients are determined experimentally. Once $\Phi(z_1)$ and $\Psi(z_2)$ are fully evaluated, the individual displacements are known from Eqs. 12.3 through 12.4. For a significantly large region of interest in a finite structure, it may also be necessary to satisfy other boundary conditions at discrete locations.

Conformal mapping is introduced to simplify the plane problem by mapping the region R_z of a complicated physical $z = x + iy$ plane of a loaded component into a region R_ζ of a simpler shape in the $\zeta = \xi + i\eta$ plane, the latter being a unit circle if one represents the stress function as a Laurent series, Fig. 12.1 [13–21]. The new coordinate system (and resulting geometry) is usually chosen to aid in solving the equations and the obtained solution from this simplified domain can then be mapped back to the original physical geometry for a valid solution.

Assume that a mapping function of the form $z = \omega(\zeta)$ exists and which maps R_ζ of the simpler plane into R_z of the more complicated physical plane. For orthotropy, auxiliary planes and their induced mapping functions are defined in terms of $\zeta_j = \xi + \mu_j \eta$, therefore $z_j = \omega_j(\zeta_j)$, for $j = 1, 2$. The induced conformal mapping functions are one-to-one and invertible. The

Fig. 12.1 Mapping circular cutout in the physical z -plane into exterior region of a unit circle in ζ -plane



stress functions $\Phi(z_1)$ and $\Psi(z_2)$ can be expressed as the following analytic functions of ζ_1 and ζ_2 . Derivatives of the stress functions with respect to their argument are

$$\Phi'(z_1) = \Phi'(\zeta_1) \frac{d\zeta_1}{dz_1} = \frac{\Phi'(\zeta_1)}{\omega_1(\zeta_1)}, \quad \Psi'(z_2) = \frac{\Psi'(\zeta_2)}{\omega_2(\zeta_2)} \quad (12.6)$$

The analyticity of the mapping functions satisfies the equilibrium and compatibility throughout region R_z of the physical plane.

12.2.1 Traction-Free Boundaries

Using the concept of analytic continuation, the individual stress functions for a region R_ζ adjacent to a traction-free boundary of the unit circle of an orthotropic material are related by [23, 24]

$$\Psi(\zeta_2) = \overline{B\Phi\left(1/\bar{\zeta}_2\right)} + C\Phi(\zeta_2) \quad (12.7)$$

where B and C are

$$B = \frac{\bar{\mu}_2 - \bar{\mu}_1}{\mu_2 - \bar{\mu}_2}, \quad C = \frac{\bar{\mu}_2 - \mu_1}{\mu_2 - \bar{\mu}_2} \quad (12.8)$$

Equation (12.7) enable the displacements of the structure to be expressed in terms of a single stress function, $\Phi(\zeta_1)$, the latter which can be represented by a Laurent series expansion. Equation (12.7) assumes ability to map the physical boundary of interest into the unit circle in the mapped plane. Reference [25] contains a simple, clear derivation of Eq. (12.7).

12.2.2 Mapping Formulation

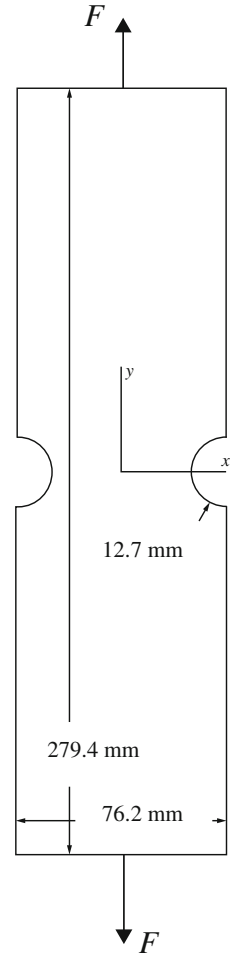
For a region adjacent the circular notch of radius R , the following function [19]

$$z_j = \omega_j(\zeta_j) = \frac{R}{2} \left[(1 - i\mu_j) \zeta_j + \frac{1 + i\mu_j}{\zeta_j} \right], \quad j = 1, 2 \quad (12.9)$$

maps the region of the exterior of a unit circle, R_ζ , of the ζ -plane into the region R_z of the z -physical plane, Fig. 12.2. The inverse of the induced mapping function is

$$\zeta_j = \omega_j^{-1}(z_j) = \frac{z_j \pm \sqrt{z_j^2 - R^2(1 + \mu_j^2)}}{R(1 - i\mu_j)}, \quad j = 1, 2 \quad (12.10)$$

Fig. 12.2 Vertically-loaded finite Gr/E [0₁₃/90₅/0₁₃] composite plate with circular side notches



The branch of the square root in Eq. (12.10) is chosen such that $|\zeta_j| \geq 1$ for $j = 1, 2$.

12.2.3 Mapping Collocation and Displacements

The single stress function can be expressed as the following finite Laurent series [17]

$$\Phi(\zeta_1) = \sum_{\substack{j=-N \\ j \neq 0}}^N A_j \zeta_1^j \quad (12.11)$$

where $A_j = a_j + ib_j$ are the unknown complex coefficients (a_j and b_j are both real numbers). The $j = 0$ term contributes to rigid-body motion and can be omitted. Substituting Eq. (12.11) into (12.7) yields

$$\Psi(\zeta_2) = \sum_{\substack{j=-N \\ j \neq 0}}^N (\bar{A}_j B \zeta_2^{-j} + A_j C \zeta_2^j) \quad (12.12)$$

where \bar{A}_j is the complex conjugate of A_j . At least for a finite, simply connected region R_ζ , $\Phi(\zeta_1)$ is a single-valued analytic function. Orthotropic composite whose complex parameters are purely imaginary when the directions of material symmetry are parallel and perpendicular to the applied load require that only odd terms be retained in the Laurent expansions. From Eqs. (12.3) and (12.4), the displacements can be written as

$$u = 2 \sum_{\substack{j = -N, -N+2, \dots \\ j \neq 0}}^N \operatorname{Re} \{ [p_1 \zeta_1^j + p_2 C \zeta_2^j] A_j + p_2 B \zeta_2^{-j} \bar{A}_j \} \quad (12.13)$$

$$v = 2 \sum_{\substack{j = -N, -N+2 \\ j \neq 0}}^N \operatorname{Re} \{ [q_1 \zeta_1^j + q_2 C \zeta_2^j] A_j + q_2 B \zeta_2^{-j} \bar{A}_j \} \quad (12.14)$$

The only unknowns in these expressions for the displacements are the complex coefficients $A_j = a_j + ib_j$, the other quantities involve geometry (location) or material properties. Because the summation in Eqs. (12.13) through (12.14) involves only the odd values of N , the number of complex coefficients, A_j , is $N + 1$ and the number of real coefficients, a_j and b_j , is $2(N + 1)$. These coefficients can be determined from measured displacement data. It should be noted that by using conformal mapping and analytic continuation techniques, Eqs. (12.13) through (12.14) imply that the induced stresses satisfy equilibrium and traction-free conditions in the adjacent portion of the entire boundary. However, unlike a classical boundary-value problem where one would typically evaluate the unknown coefficients, A_j , by satisfying the boundary and loading conditions around the entire shape, one can use a combination of the measured stresses and/or displacements from within region R_z to determine these unknown complex coefficients, A_j . Additional known boundary conditions may also be imposed at discrete locations. The concept of collecting measured data in a region R^* adjacent to an edge Γ , mapping R_z into R_ζ such that Γ of the physical z -plane is mapped into the unit circle in the ζ -plane whereby the traction-free conditions on Γ are satisfied continuously, relating the two complex stress functions to each other, plus satisfying other loading conditions discretely on the boundary of the component beyond Γ will be referred to as the mapping-collocation technique.

The interior displacement data v^* at m different locations within region R^* and q known stress conditions (in terms of σ_{xy}) at discrete points along the free outer surface and line of symmetry ($y = 0$) are employed. A system of simultaneous linear equations $[V]_{(m+q) \times 2(N+1)} \{c\}_{2(N+1) \times 1} = \{V^*\}_{(m+q) \times 1}$, is formed whose matrix $[V]$ consists of analytical expressions of displacement component v^* , Eq. (12.14), and the expressions of the known stress conditions, vector $\{c\} = \{a_{-N}, b_{-N}, a_{-N+2}, b_{-N+2}, \dots, a_{N-2}, b_{N-2}, a_N, b_N\}$ has $2(N + 1)$ unknown real coefficients, and vector $\{V^*\}$ includes the m measured displacement values of v^* and q discretely imposed stress conditions such that $m + q \gg N + 1$. The best values of the coefficients A_j , in a least-squares numerical sense, can then be determined. The variables $\zeta_j = \xi + \mu_j \eta$ are related to the physical locations $z = x + iy$ through the inverse mapping function $z_j = \omega_j(\zeta_j)$ of Eqs. (12.9) through (12.10).

12.2.4 Inverse Method Procedure

The particular inverse method used here is combining displacement produced from Airy stress function scheme with displacements measured using DIC. Through an iterative process that determines new constitutive parameters, the displacement difference between measured DIC and produced from Airy stress function is minimized. The function to be minimized is

$$f(\hat{v}_{Airy}, P) = \|r\|, \quad \text{where } r = \hat{v}_{DIC} - \hat{v}_{Airy} \quad (12.15)$$

where \hat{v}_{Airy} and \hat{v}_{DIC} are vector containing nodal v -displacements determined by Airy stress function scheme and DIC, respectively. P is a vector containing the constitutive parameters, $E_1, E_2, \nu_{12}, G_{12}$ and $\|r\|$ is the norm of r . Because Eq. (12.15) is nonlinear with respect to P , iterative procedures are appropriate methods for minimizing of $f(\hat{v}_{Airy}, P)$ and determination of P . LMA (Levenberg-Marquardt Algorithm) is commonly used because it combines the benefits of Steepest Descent Method and Gauss-Newton Method. The LMA has the form [15]

$$P_{i+1} = P_i - (J^T J + \lambda \cdot \text{diag}(J^T J))^{-1} J^T r \quad (12.16)$$

where i is iteration number, J and J^T are Jacobian and Jacobian transpose, determined by backward difference, $J_{m,n} = \frac{\partial r_m}{\partial P_n}$; m is number of nodal displacements and n is number of constitutive parameters (4 in this work), and λ is non-negative damping factor, adjusted each iteration step, adjusts between Steepest Descent Method and Gauss-Newton Method.

The primary disadvantage of LMA is the need for matrix inversion during each iteration. In most applications, reduced iterations compensate for the matrix inversion.

After calculating a new P_{i+1} , the constitutive parameters are checked for validity, i.e., a positive-definite stiffness matrix, and are adjusted if not valid. The validated P_{i+1} are inputs to a new analysis and the resulting nodal displacements are used to determine f_{i+1} . If $f_{i+1} < f_i$, the constitutive parameters are updated, $P_{i+1} \rightarrow P_i$, λ is reduced by a factor of 10, and the next iterations begins. If $f_{i+1} > f_i$, then λ is increased by a factor of 10 and P_i is not updated. As $\lambda \rightarrow 0$, LMA becomes exactly the Gauss-Newton Method.

12.3 Experimental Details

The developed inverse hybrid-DIC approach is utilized to analyze a finite-width tensile $[0_{13}/90_5/0_{13}]$ graphite/epoxy orthotropic plate (from Kinetic Composites, Inc., Oceanside, CA; $E_1 = 104$ GPa, $E_2 = 28$ GPa, $G_{12} = 2.9$ GPa, $\nu_{12} = 0.16$ [1]) with side notches of radius $R = 12.7$ mm was loaded in the strongest/stiffest material direction (1-, y-direction), Fig. 12.2. Over-all laminate dimensions are 279.4 mm long, 76.2 mm wide and 5.28 mm thick. The side notches were machined with a water jet. The coordinate origin is at the center of the plate and the response is symmetric about x - and y -axes. The laminate elastic properties were obtained from conducting uniaxial tensile tests in the strong/stiff (y-direction), weak/compliant (x-direction) and 45-degree orientations [1].

12.3.1 Digital Image Correlation

Digital Image Correlation (DIC) is a full-field computer-based image analysis technique for the non-contact measurement of displacements of a surface equipped with a speckle pattern. The method tracks the motion of the speckles by comparing the gray scale value at a point (subset) in a deformed and undeformed configuration. Two sets of images are recorded; the first image typically being at zero load and the second image under load. Vic-Snap software (by Correlated Solutions, Inc., Columbia, SC, USA) was used to record the images of the plate in its loaded and unloaded conditions and to evaluate the displacements for post-processing. When utilizing two cameras, a separate calibration grid (provided by Correlated Solution with the DIC package) was used to evaluate the displacement data in physical units rather than in pixels. Quality displacement information at and near the edge of the notch and at (near) the longitudinal edge of the specimen is unavailable because the DIC software's correlation algorithm is unable to track a group of pixels (subset) which lack neighboring pixels. To perform the tracking, the subset is shifted until the pattern in the deformed image closely matches that of the reference image.

The measured DIC data were digitalized in matrix form and combined with the Airy stress function to determine the constitutive properties. Recognizing one has fewer complex coefficients to evaluate than amount of data from which to evaluate them, the coefficients were determined using least squares. Although the recorded displacement data at, and adjacent to, an edge are unreliable and raw displacement information in composites is inherently noisy, the present technique overcomes these challenges by avoiding the use of recorded data on and near edges and by processing the measured interior data with a stress function, mapping and analytic continuation.

12.3.2 Plate Preparation and Data Recording and Processing

A random speckle pattern of white dots on a black background was applied to the composite's surface. The plate was statically loaded in the hydraulic grips of a 20 kips capacity MTS hydraulic testing machine from 0 N to 7,117 N in 890 N load increments. Displacement data were recorded and processed at each load increment. Before conducting the quantitative analysis, two cameras were used to capture the three displacement components by which to verify there was no out-of-plane

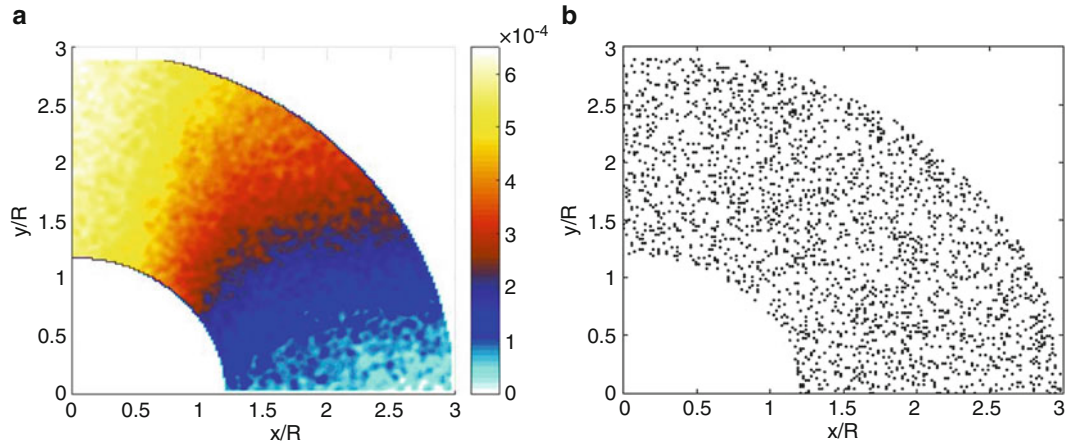


Fig. 12.3 (a) Averaged recorded v -displacement data from Vic-snap from all four quadrants; (b) Source locations of $m = 2,200$ DIC values

bending [1]. The recorded v -displacement information was exported to MATLAB (Mathworks, Inc. 2015) to convert each pixel into a data point, i.e., points. Since DIC data typically are unreliable on and near an edge, no recorded displacements were used within at least $2.95 \text{ mm} = 0.12 \text{ in.}$ of the boundary of the notch.

The DIC correlated solution software provided approximately 102,200 values of v when the analysis was carried out for 17 subsets in five steps. The plate is geometrically and mechanically symmetrical about the vertical y -axes. Since the top end of the physically tested plate was fixed stationary while the bottom end moved vertically downward, the zero vertical displacement was shifted to be at the horizontal middle of the plate to represent the case of the plate being extended at both top and bottom ends. The measured v -displacement data were subsequently averaged about all quadrants to cancel any asymmetry and the resulting averaged measured values of 17,666 v -displacement data are plotted in the second quadrant as shown in Fig. 12.3a. For the subsequently used mathematical mapping, the coordinate origin was also transferred to the center of the left notch. Due to the previously mentioned unreliability, recorded data on and near the edge of the notch were not employed. Only 2,200 of the available 17,666 v -displacements were selected randomly and used. Their source locations are shown in Fig. 12.3b. The region of Fig. 12.3b is denoted as region R^* . Like most experimental data, the measured data incorporate some noise which necessitate collecting more measured input values than the number of unknown coefficients of a stress function. In addition to the selected v -displacements associated with Fig. 12.3b, $\sigma_{xy} = 0$ was imposed at each of 12 equally-spaced discrete locations along the left vertical traction-free edge of the plate and along the horizontal line of symmetry, $y = 0$. The total number of equations (side conditions), $m + q$, where $m = 2,200$ and $q = 24$, exceeds the number of real coefficients, $2(N + 1)$, producing an overdetermined system which can be solved using a least-squares. The system was solved in MATLAB using the backslash ‘\’ operator.

12.3.3 Evaluating Number of Coefficients to Employ

The coefficients, $A_j = a_j + ib_j$, were evaluated using Eqs. (12.9) through (12.10) to map the physical plane into the unit circle in the ζ -plane. The unreliable v -displacement values on and near the boundary of the side notch motivated using only v -displacements originating at locations shown in Fig. 12.3b. The magnitude of the complex coefficients, A_j , were determined from Eq. (12.14) using the measured v -displacement data located inside the region R^* , Fig. 12.3b, and imposing zero shear stress discretely along the outer left vertical free surface and the line of symmetry, $y = 0$. The number of real coefficients, $2(N + 1)$, to retain was selected to be 6 complex (12 real) coefficients [1].

12.4 Results

Table 12.1 shows the calculated values of constitutive parameters using Airy stress function scheme and DIC displacement data. LMA requires two initial estimates of P in order to calculate J and begin iterations. Genovese et al. [14] evaluated the

Table 12.1 Calculated values of constitutive properties using inverse method and airy stress function scheme

Parameters	First initial guess	% error	Second initial guess	% error	Calculated values	Final % error
E_1 (GPa)	181	80.0%	110	10.0%	103	2.9%
E_2 (GPa)	39.8	60.0%	22.4	20.0%	22.3	10.4%
G_{12} (GPa)	4.61	60%	2.59	20.0%	2.58	10.4%
ν_{12}	0.167	10%	0.122	20.0%	0.140	7.9%

Target values of elastic constants are $E_1 = 101$ GPa, $E_2 = 24.9$ GPa, $G_{12} = 2.88$ GPa, $\nu_{12} = 0.152$ [1]

effect of initial estimates on the number of iterations using FEMU-U in an overdetermined system and found that poor initial estimates increased the iterations required for minimization, but minimization was eventually achieved. Although evaluation of initial estimates is beyond the scope of this investigation, an informal analysis showed lack of convergence for poor initial estimates, primarily because the rate of convergence was different of each constitutive parameters.

12.5 Summary, Discussion and Conclusions

A new inverse problem formulation is developed using the Airy stress function, Levenberg-Marquardt Algorithm, and DIC measured displacement to determine the constitutive properties of a graphite/epoxy laminated composite loaded vertically. The primary advantage of this new formulation is the direct use of displacement data, eliminating the need for numerical differentiation when strain data is required. The inverse method algorithm determined the constitutive properties with errors range from 2% to 10%.

References

- Alshaya, A.A.: Experimental, analytical and numerical analyses of orthotropic materials and biomechanics application. PhD thesis, University of Wisconsin-Madison (2017)
- Alshaya, A., Rowlands, R.: Experimental stress analysis of a notched finite composite tensile plate. *Compos. Sci. Technol.* **144**, 89–99 (2017). ISSN 0266-3538, <http://dx.doi.org/10.1016/j.compscitech.2017.03.007>. (<http://www.sciencedirect.com/science/article/pii/S0266353816312143>)
- Ju, S.H., Rowlands, R.E.: Thermoelastic determination of KI and KII in an orthotropic graphite–epoxy composite. *J. Compos. Mater.* **37**(22), 2011–2025 (2003)
- Ju, S.H., Rowlands, R.E.: Mixed-mode thermoelastic fracture analysis of orthotropic composites. *Int. J. Fract.* **120**(4), 601–621 (2003)
- Lin, S.T., Rowlands, R.E.: Thermoelastic stress analysis of orthotropic composites. *Exp. Mech.* **35**(3), 257–265 (1995)
- Alshaya, A., Shuai, X., Rowlands, R.: Thermoelastic stress analysis of a finite orthotropic composite containing an elliptical hole. *Exp. Mech.* **56**(8), 1373–1384 (2016)
- Rhee, J., Rowlands, R.E.: Thermoelastic-numerical hybrid analysis of holes and cracks in composites. *Exp. Mech.* **39**(4), 349–355 (1999)
- Hawong, J.S., Lin, C.H., Lin, S.T., Rhee, J., Rowlands, R.E.: A hybrid method to determine individual stresses in orthotropic composites using only measured isochromatic data. *J. Compos. Mater.* **29**(18), 2366–2387 (1995)
- Baek, T.H., Rowlands, R.E.: Experimental determination of stress concentrations in orthotropic composites. *J. Strain Anal. Eng. Des.* **34**(2), 69–81 (1999)
- Baek, T., Rowlands, R.: Hybrid stress analysis of perforated composites using strain gages. *Exp. Mech.* **41**(2), 195–203 (2001)
- Avril, S., Pierron, F.: General framework for the identification of constitutive parameters from full-field measurements in linear elasticity. *Int. J. Solids Struct.* **44**(14–15), 4978–5002 (2007)
- Le Magorou, L., Bos, F., Rouger, F.: Identification of constitutive laws for wood-based panels by means of an inverse method. *Compos. Sci. Technol.* **62**(4), 591–596 (2002)
- Molimard, J., Le Riche, R., Vautrin, A., Lee, J.-R.: Identification of the four orthotropic plate stiffnesses using a single open-hole tensile test. *Exp. Mech.* **45**(5), 404–411 (2005)
- Genovese, K., Lamberti, L., Pappalettere, C.: Improved global–local simulated annealing formulation for solving non-smooth engineering optimization problems. *Int. J. Solids Struct.* **42**(1), 203–237 (2005)
- Considine, J.M., Vahey, D.W., Matthys, D., Rowlands, R.E., Turner, K.T.: An inverse method for analyzing defects in heterogeneous materials. In: Proulx, T. (ed.) *Application of Imaging Techniques to Mechanics of Materials and Structures, Volume 4: Proceedings of the 2010 Annual Conference on Experimental and Applied Mechanics*, pp. 339–346. Springer New York, New York (2013)
- Lekhnitskii, S.G.: *Anisotropic Plates*. Gordon & Breach Scientific Publishers, New York (1968)
- Bisshopp, F.: Numerical conformal mapping and analytic continuation. *Q. Appl. Math.* **41**, 125–142 (1983)
- Challis, N.V., Burley, D.M.: A numerical method for conformal mapping. *IMA J. Numer. Anal.* **2**(2), 169–181 (1982)
- Lekhnitskii, S.G.: *Theory of Elasticity of an Anisotropic Elastic Body*. Holden-Day, San Francisco (1963)

20. Lin, S.T., Rowlands, R.E.: Hybrid stress analysis. *Opt. Lasers Eng.* **32**(3), 257–298 (1999)
21. Muskhelishvili, N.: *Some Basic Problems of the Mathematical Theory of Elasticity*. Springer, Leyden (1977)
22. Savin, G.N.: *Stress Concentration Around Holes*. Pergamon Press 1961
23. Bowie, O.L., Freese, C.E.: Central crack in plane orthotropic rectangular sheet. *Int. J. Fract. Mech.* **8**(1), 49–57 (1972)
24. Gerhardt, T.D.: A hybrid/finite element approach for stress analysis of notched anisotropic materials. *J. Appl. Mech.* **51**(4), 804–810 (1984)
25. Huang, Y.-M.: Determination of individual stresses from thermoelastically measured trace of stress tensor. PhD thesis, University of Wisconsin-Madison